STEADY-STATE AND DYNAMIC MODELS OF UNIFIED POWER FLOW CONTROLLER (UPFC) FOR POWER SYSTEM STUDIES

A. Nabavi-Niaki M.R. Iravani
Department of Electrical and Computer Engineering
University of Toronto
Toronto, Ontario M5S 1A4
Canada

Abstract: This paper provides comprehensive development procedures and final forms of mathematical models of unified power flow controller (UPFC) for steady-state, transient stability and eigenvalue studies. Based on the developed models, the impacts of control strategy, parameters and location of UPFC on power system operating conditions are discussed. The accuracy of the developed models is verified through comparing the study results with those obtained from detailed time-domain simulation using the Electromagnetic Transients Program (EMTP).

Keywords: Modelling; FACTS; UPFC, Eigen Analysis; Steady-State Analysis, Transient Stability Analysis.

1. INTRODUCTION

Unified power flow controller (UPFC) [1,2] can be used for power flow control, loop-flow control, load sharing among parallel corridors, enhancement of transient stability, mitigation of system oscillations and voltage (reactive power) regulation. Performance analysis and control synthesis of UPFC require its steady-state and dynamic models. Reference [1] introduces a steady-state UPFC model based on a single, ideal, series voltage source. Reference [3] utilizes two ideal voltage sources, one in series and one in parallel as UPFC steady-state model. The steady-state UPFC model suggested in [4] is based upon one ideal, series voltage source, and one ideal, shunt current source. The above steady-state models are based on simplifying assumptions and consequently have various limitations. A two-source UPFC steady-state model including source impedances is suggested in [5].

The primary objective of this paper is to develop steady-state and dynamic models of UPFC for power flow analysis, transient stability investigation and eigen analysis. Typical applications of the models are presented, and where applicable the EMTP is used to verify the accuracy of the developed models.

2. UPFC MATHEMATICAL MODEL

Figure 1 shows single-phase, schematic diagram of the power circuit of a UPFC which is composed of an excitation transformer (ET), a boosting transformer (BT), two three-phase GTO based voltage source converters (VSCs), and a dc link capacitor. In Figure 1, m and δ refer to amplitude modulation index and phase-angle of the control signal of each VSC respectively. Figure 2 shows detailed three-phase circuit diagram of ET, BT and the converters. The two transformers are identified by their per phase leakage inductances and resistances. Figure 2 illustrates that each converter leg is composed of a GTO valve and a diode valve in antiparallel connection to permit bidirectional current flow.

In the case of high-voltage applications, where only GTO-converters are economical, and the switching frequency is limited to a few hundred hertz, off-line optimized pulse patterns are often selected for the converter. The pulse width modulation (PWM) approach which is used in this paper encompasses the concept of optimized pulse pattern schemes. For cost reduction and maximum converter utilization, PWM-schemes such as space-vector modulation are applied in practice. As long as the fundamental frequency components under balanced operating conditions are concerned, the space-vector approach and the general PWM approach used in this paper provide the same mathematical model.

To describe the modelling procedures, let's consider the dc link, phase 'a' of ET, and the corresponding VSC-E arms as shown in Figure 3. In Fig. 3, r_E and ℓ_E represent per phase resistance and inductance of ET. In Fig. 3, the bidirectional switches are identified by ζ_{Ea} and ζ'_{Ea} which can be either on or off. r_s is the switch on-state resistance. r_s also includes valve conduction losses in the analysis. S_{Ea} (S'_{Ea}) is defined as the switching function of switch

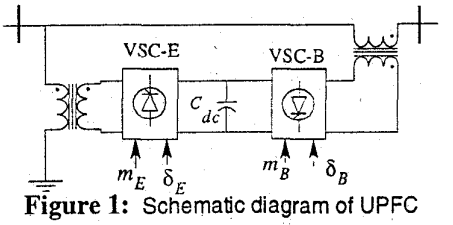

Figure 1: Schematic diagram of UPFC

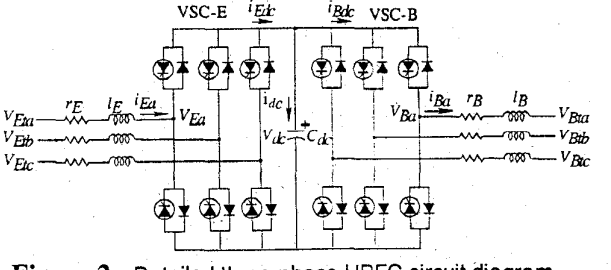

Figure 2: Detailed three-phase UPFC circuit diagram

96 WM 257-6 PWRS A paper recommended and approved by the IEEE Power System Engineering Committee of the IEEE Power Engineering Society for presentation at the 1996 IEEE/PES Winter Meeting, January 21-25, 1996, Baltimore, MD. Manuscript submitted July 28,1995; made available for printing January 10, 1996

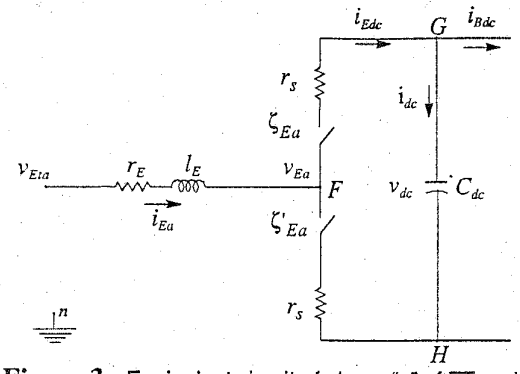

Figure 3: Equivalent circuit of phase "*a*" of ET and VSC-E.

$\zeta_{Ea}(\zeta'_{Ea})$. S_{Ea} (S'_{Ea}) is either 1 or 0 corresponding to on and off states of the switch respectively. Based upon the principle of operation of a VSC, regardless of the adopted PWM scheme, S_{Ea} and S'_{Ea} are always complementary, i.e.

$$S_{Ea} + S'_{Ea} = 1 \tag{1}$$

Thus, the behaviour of the circuit of Fig. 3 can be expressed as

$$\ell_E(di_{Ea}/dt) + r_E i_{Ea} = \upsilon_{Eta} - \upsilon_{Ea} \tag{2}$$

and

$$\upsilon_{Ea} = \upsilon_{FH} + \upsilon_{Hn} \tag{3}$$

When ζ_{Ea} is on $S_{Ea} = 1$, and $S'_{Ea} = 0$

$$\upsilon_{FH} = (i_{Ea} r_s + \upsilon_{dc}) S_{Ea} \tag{3a}$$

When ζ_{Ea} is off $S_{Ea} = 0$, and $S'_{Ea} = 1$

$$\upsilon_{FH} = (i_{Ea} r_s) S'_{Ea} \tag{3b}$$

From (3), (3a) and (3b) one can deduce

$$\upsilon_{FH} = (i_{Ea} r_s + \upsilon_{dc}) S_{Ea} + (i_{Ea} r_s) S'_{Ea} \tag{4}$$

Substituting for S'_{Ea} from (1) in (4), for υ_{FH} from (4) in (3), and finally for υ_{Ea} from (3) in (2)

$$\ell_E(di_{Ea}/dt) = -R_E i_{Ea} - (\upsilon_{dc} S_{Ea} + \upsilon_{Hn}) + \upsilon_{Ea} \tag{5}$$

where $R_E = r_E + r_s$. Equations similar to (5) for phases 'b' and 'c' can also be developed. With reference to Fig. 2, $i_{Ea} + i_{Eb} + i_{Ec} = 0$ and $\upsilon_{Eta} + \upsilon_{Etb} + \upsilon_{Etc} = 0$. Thus, voltage υ_{Hn} can be obtained by adding equations of the three phases as given by (6).

$$\upsilon_{Hn} = (-\upsilon_{dc}/3) \sum_{i=a,b,c} S_{Ei} \tag{6}$$

Substituting for υ_{Hn} from (6) in (5), the final expression for phase 'a' is deduced

$$\ell_E(di_{Ea}/dt) = -R_E i_{Ea} - \upsilon_{dc} S_{Ea} + (\upsilon_{dc}/3) \sum_{i=a,b,c} S_{Ei} + \upsilon_{Eta} \tag{7}$$

Equations similar to (7) are also developed for phases 'b' and 'c'. The main advantage of expressing (7) in terms of the generalized switching functions S_{Ea}, S_{Eb} and S_{Ec} is that it will not be dependent on the selected PWM technique. Figure 4(a) shows a generalized PWM switching pattern for S_{Ea}. The PWM patterns of S_{Eb} and S_{Ec} are identical to that of Fig. 4a with appropriate phase shifts. In Fig. 4, the fundamental frequency of the VSC is ω, the frequency of the switching function is ω_s, and $\bar{d}_{Ea}$ is the average of S_{Ea} within one period corresponding to the switching frequency. Since S_{Ea} is a discrete, periodic function of time, its Fourier series can be expressed as

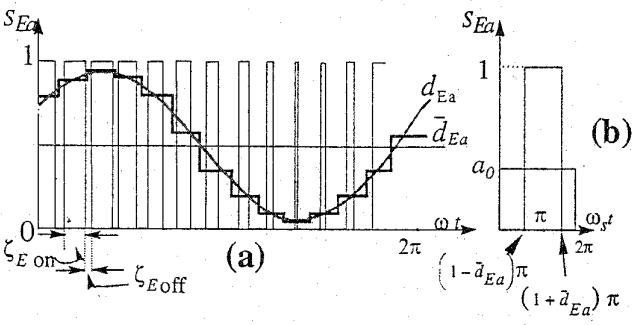

Figure 4: (a) A generalized PWM pattern for phase "*a*", (b) Switching function S_{Ea} and its average value a_0 in one switching period.

$$S_{Ea} = a_o + \sum_n b_n \cos(n\omega t) \tag{8}$$

where $a_o = \bar{d}_{Ea}$ and $b_n = (-1)^n (2/n\pi) \sin(n\pi \bar{d}_{Ea})$

Figure 4(a) also shows variations of $\bar{d}_{Ea}$ within one period corresponding to the system fundamental frequency. The fundamental component of $\bar{d}_{Ea}$ in Fig. 4(a), which is referred to as the control signal, is expressed as

$$d_{Ea} = (m_E/2)\cos(\omega t - \delta_E) + \tfrac{1}{2} \tag{9}$$

d_{Eb} and d_{Ec} for phases 'b' and 'c' are identical to (9) except for phase shifts of $2\pi/3$ and $4\pi/3$ respectively. Thus υ_{Hn} can be calculated from (6) by substituting for S_{Ei}'s in terms of d_{Ea}, d_{Eb} and d_{Ec} (note that only the fundamental component is considered). Then the calculated υ_{Hn} and υ_{FH} are substituted in (3) to derive the final expression for υ_{Ea}

$$\upsilon_{Ea} = (m_E \upsilon_{dc}/2)\cos(\omega t - \delta_E) = A_E \cos\theta_E \tag{10}$$

Final expression for υ_{Eb} and υ_{Ec} are identical to (10), except for phase shifts of $2\pi/3$ and $4\pi/3$. Therefore, with respect to its ac terminals, at the fundamental frequency, VSC-E is equivalent to a three-phase, balanced, controlled, voltage source expressed by υ_{Ea}, υ_{Eb}, and υ_{Ec}. Amplitude, phase-angle and frequency of the three-phase voltage source are controlled by m_E, δ_E and ω of the control signal (Fig. 4(a)). The mathematical model which governs the behaviour of phase 'a' is obtained by substituting for υ_{Ea} from (10) in (2).

$$\ell_E(di_{Ea}/dt) = -R_E i_{Ea} - A_E \cos\theta_E + \upsilon_{Eta} \tag{11}$$

Similar expressions to that of (11) for phases 'b' and 'c' are also deduced.

The mathematical procedures described by (1)-(10) and the mathematical model of (11) are also applicable for VSC-B and the boosting transformer of Fig. 2. Thus the overall mathematical model of VSC-E, VSC-B, ET and BT of Fig. 2 is expressed by matrix equation

$$L(di/dt) = -Ri + Q + \upsilon \qquad (12)$$

where

$L = diag[\ell_E \ell_E \ell_E \ell_B \ell_B \ell_B]$

$i = [i_{Ea} i_{Eb} i_{Ec} i_{Ba} i_{Bb} i_{Bc}]$

$R = diag[R_E R_E R_E R_B R_B R_B]$

$\upsilon = [\upsilon_{Eta} \upsilon_{Etb} \upsilon_{Etc} - \upsilon_{Bta} - \upsilon_{Btb} - \upsilon_{Btc}]$

$Q = diag[-A_E \cos\theta_E - A_E \cos(\theta_E - 2\pi/3) - A_E \cos(\theta_E - 4\pi/3)$

$A_B \cos(\theta_B) A_B \cos(\theta_B - 2\pi/3) A_B \cos(\theta_B - 4\pi/3)]^T$

$A_E = m_E \upsilon_{dc}/2, A_B = m_B \upsilon_{dc}/2$

The dynamics of the dc link capacitor, Fig. 2, is

$$d\upsilon_{dc}/dt = (1/c_{dc}) i_{dc} \qquad (13)$$

where i_{dc} in terms of the defined switching functions is

$$i_{dc} = i_{Edc} - i_{Bdc} = \sum_{j=a,b,c} (i_{Ej} d_{Ej} - i_{Bj} d_{Bj}) \qquad (14)$$

Equation (14) demonstrates that the effect of each switching converter on the dc link can be expressed by a current source. Therefore, the generalized equivalent circuit of the UPFC, based on (12) and (13), can be illustrated by Fig. 5. Based on (12) and (13), a state space representation of the UPFC is

$$\dot{x} = A_g x + B_g u \qquad (15)$$

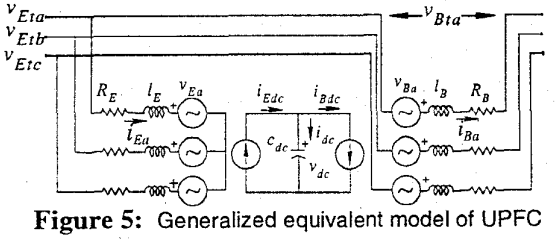

Figure 5: Generalized equivalent model of UPFC

where $x = [i_{Ea} i_{Eb} i_{Ec} i_{Ba} i_{Bb} i_{Bc} \upsilon_{dc}]^T$

$u = [\upsilon_{Eta} \upsilon_{Etb} \upsilon_{Etc} - \upsilon_{Bta} - \upsilon_{Btb} - \upsilon_{Btc} 0]^T$

Elements of A_g and B_g are given in Appendix A. The UPFC mathematical model given by (15) is valid for the frequency range less than the switching frequency ω_s (Fig. 4).

2.1 UPFC Steady-State Model

Neglecting UPFC losses, during steady-state operation it neither absorbs nor injects real power with respect to the system. Physical interpretation of this statement is that the voltage of the dc link capacitor remains constant at the pre-specified value V_{dc}. This constraint must be satisfied by the UPFC steady-state equations. Thus, the UPFC steady-state model is deduced from (15) as

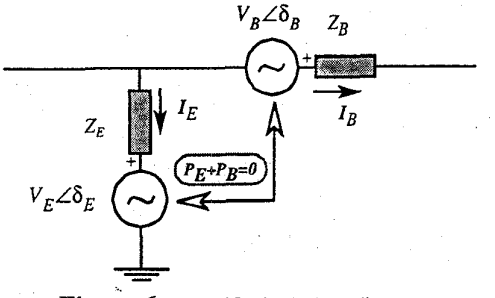

Figure 6: UPFC single line diagram .

$$0 = \begin{bmatrix} -Z_E & & & & & & \\ & -Z_E & & & & & \\ & & -Z_E & & & & \\ & & & -Z_B & & & \\ & & & & -Z_B & & \\ & & & & & -Z_B & \\ & & & & & & -Z_B \end{bmatrix} \begin{bmatrix} I_{Ea} \\ I_{Eb} \\ I_{Ec} \\ I_{Ba} \\ I_{Bb} \\ I_{Bc} \end{bmatrix} + \begin{bmatrix} V_{Eta} - V_{Ea} \\ V_{Etb} - V_{Eb} \\ V_{Etc} - V_{Ec} \\ V_{Ba} - V_{Bta} \\ V_{Bb} - V_{Btb} \\ V_{Bc} - V_{Btc} \end{bmatrix} \qquad (16)$$

where $Z_E = R_E + j\omega L_E, Z_B = R_B + j\omega L_B$

$V_{Ei} = (M_E V_{dc}/2\sqrt{2}) \angle \delta_E, V_{Bi} = (M_B V_{dc}/2\sqrt{2}) \angle \delta_B, (i = a,b,c)$

M_E, M_B and V_{dc} are the steady-state values of m_E, m_B and υ_{dc}. I_{Ei}'s and I_{Bi}'s are phasors of the line currents (Fig. (2)).

Based on (16), the UPFC single line diagram under a steady-state condition is given by Fig. 6. The constraint $P_B + P_E = 0$ in Fig. 6 implies that:

- no real-power is exchanged between the UPFC and the system, thus the dc link voltage remains constant (losses neglected),
- and the two sources are mutually dependent.

Depending upon the UPFC control strategy and function, its various power flow models can be deduced from (16) and Fig. 6 as follows.

2.1.1 UPFC Power Flow Model

Let's consider the UPFC of Fig. 7(a) which is used to maintain a pre-specified power flow from E-bus to B-bus, and to regulate the B-bus voltage at a specific value. Using power flow terminology, B-bus is a P-V bus and E-bus is a

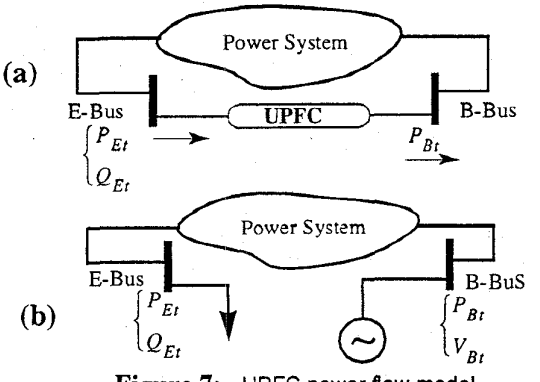

Figure 7: UPFC power flow model

P-Q bus, Fig. 7(b). Neglecting UPFC losses, $P_{Bt} = P_{Et}$ = pre-specified value. δ_B and M_B determine P_{Bt} (as well as P_{Et}) and V_{Bt} respectively. M_E and δ_E determine Q_E and V_{dc} respectively. To calculate the UPFC control variable for the given power flow condition, a power flow analysis is performed where the UPFC is modelled as given in Fig. 7(b). Then, the power flow analysis results are used to solve the UPFC steady-state equations to determine δ_B, M_B, δ_E and M_E.

$$F - S = 0 \tag{17}$$

where $F = [f_1(P_{Et}) f_2(Q_{Et}) f_3(P_{Bt}) f_4(Q_{Bt})]^T$

$S = [P_{Et}\, Q_{Et}\, P_{Bt}\, Q_{Bt}]^T$

f_1 to f_4 are nonlinear functions which are deduced from the UPFC steady-state model and Fig. 6. f_1 to f_4 are also given in Appendix A. Equation (17) is nonlinear and its solution best obtained by an iterative numerical approach as

$$u^{k+1} = u^k + j^{-1}\Delta S \tag{18}$$

where $u = [\delta_B\, M_B, \delta_E\, M_E]^T$

$\Delta S = F - S$ and j is the Jacobian matrix.

2.2 UPFC Dynamic Model

Dynamic model of the power circuit of a UPFC in the abc (stator) reference frame is also given by (15). The extended Park's transformation matrix of (19) is used to develop time-invariant form of (15) in a two-axis (d-q-o) rotating reference frame as given by (20).

$$T = diag[P \quad P \quad 2/3] \tag{19}$$

where P is the 3×3 Park's transformation matrix [6].

$$\dot{x}_{dqo} = A_{dqo} x_{dqo} + B_{dqo} \upsilon_{dqo} \tag{20}$$

where $x_{dqo} = [i_{Ed} i_{Eq} i_{Eo} i_{Bd} i_{Bq} i_{Bo} v_{dco}]^T$

$\upsilon_{dqo} = [\upsilon_{Etd} \upsilon_{Etq} \upsilon_{Eto} \upsilon_{Btd} \upsilon_{Btq} \upsilon_{Bto} 0]^T$

Elements of matrices A_{dqo} and B_{dqo} are also given in Appendix A.

2.2.1 UPFC Transient Stability Model

Conventionally, for transient stability studies, except the electrical circuits of synchronous machine rotors and some controllers, the electrical network is represented by their algebraic phasor equations. Thus the power circuitry of a UPFC for transient stability studies can be represented by the phasor equivalent of Fig. 6. However, during transient studies, the dc link capacitor of UPFC will exchange energy with the system and consequently its voltage varies. Thus for transient stability studies the constraint $P_E + P_B = 0$ does not apply. Variation of the dc link voltage is determined by the UPFC controls and their limits. The UPFC controls and the corresponding limits are represented as nonlinear differential equations for transient stability studies.

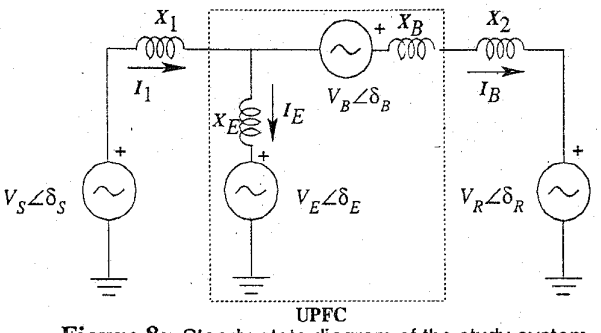

Figure 8: Steady-state diagram of the study system.

2.2.2 UPFC Small-Signal Dynamic Model

For the purpose of eigen analysis, e.g. torsional oscillations and UPFC controller design, a small-signal model of the UPFC in a d-q reference frame can be developed from linearization of (20) about an operating point.

$$\Delta \dot{x}_{dqo} = A\Delta x_{dqo} + B\Delta u \tag{21}$$

where $\Delta x_{dqo} = [\Delta i_{Ed} \Delta i_{Eq} \Delta i_{Eo} \Delta i_{Bd} \Delta i_{Bq} \Delta i_{Bo} \Delta v_{dc}]^T$

$\Delta u = [\Delta m_E \Delta m_B \Delta\delta_E \Delta\delta_B]^T$

Elements of A and B are also given in Appendix A.

It should be noted that (21) is accurate for the analysis of small-signal dynamics in the frequency range lower than the switching frequency ($\omega_s = 2nf_s$) adopted for the UPFC. Since the UPFC switching frequency is usually in the range of 300 Hz to 500 Hz, the small-signal model of (21) can be used for investigation of a wide variety of system dynamics, e.g. low-frequency (0.1-2 Hz) electromechanical modes, torsional oscillatory modes (5-55 Hz), and second and third harmonic resonances. It should be noted that the UPFC model of (21) does not include the effect of harmonics generated by the switching strategy. Therefore, if the switching pattern results in harmonics which are of significance with respect tto small-signal dynamics, e.g. third harmonic, equation (21) cannot accurately represent the UPFC behaviour. Equation (21) can be simplified if only low frequency (0.1-2 Hz) electromechanical modes of the system are of interest.

3. APPLICATION EXAMPLES AND MODEL VERIFICATION

Based upon the mathematical models developed in Section 2, this section demonstrates some of the impacts of the UPFC parameters and control functions on the operation of power systems. This section also verifies the accuracy of the UPFC models through comparison of the study results with those obtained from EMTP studies.

3.1 Steady-State

A 500 kV radial transmission line equipped with a UPFC is used for the studies. Figure 8 shows equivalent single-line diagram of the system. The UPFC regulates the power flow by adjusting magnitude ($|V_B|$) and/or phase-angle (δ_B) of the injected voltage. This mode of operation of the UPFC is that of a static phase-shifter [2].

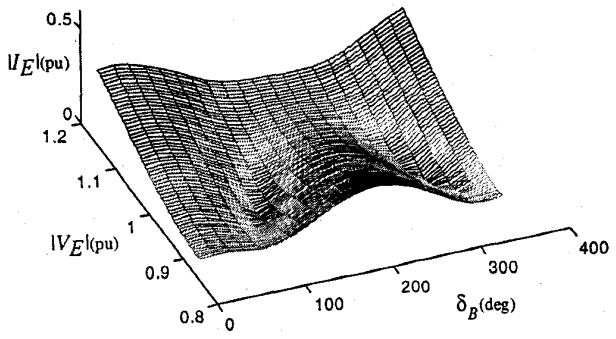

Figure 9: Range of variation of $|I_E|$ ($|V_B| = 0.5$pu)

3.1.1 Case-1

The UPFC is located at the middle of the line, i.e. x_1=x_2+x_B=0.5 per unit. $|V_B|$ and δ_B can be adjusted from 0 to 0.5 per unit and 0° to 360° respectively. $|V_E|$ can be regulated from 0.9 to 1.1 per unit. Initially power angle $(\delta = \delta_S - \delta_R)$ is adjusted at 35°. Figure 9 shows the range of variations of $|I_E|$ as a function of $|V_E|$ and δ_B when $|V_B|$ =0.5 per unit. Figure 9 illustrates that:

- Variation of electrical quantities (e.g. $|I_E|$) as a result of UPFC control strategy (e.g. control of $|V_B|$, $|V_E|$ and δ_B) is highly nonlinear and multiple-valued.
- Proper selection of the UPFC parameters and control strategy can confine the variations within acceptable limits (e.g. $0.0 < |I_E| < 0.5$). Studies similar to that of Fig. 9 identifies maximum steady-state values of the UPFC variables and determines the steady-state ratings of the UPFC components.

3.1.2 Case-2

Figure 10 shows the impact of the UPFC on the sending-end and receiving-end complex powers of the study system. The UPFC is located at the middle of the line. For each value of $|V_B|$ from 0 to 0.5 per unit, δ_B is varied from 0° to 360°. $|V_E|$ is adjusted at 1.0 per unit. Figure 10 shows that for each value of power transfer (P_o) through the line:

- there can be more than one value of reactive power exchange at each terminal, and
- the magnitude and direction of reactive power flow at each end depend on the UPFC variables, i.e. $|V_B|$, $|V_E|$ and δ_B.

The shaded areas in Fig. 10 identify minimum reactive power exchange at the line terminals corresponding to a set of UPFC selected variables. By controlling $|V_E|$, the UPFC can control Q_S and Q_R. Thus, the complex power regions of Fig. 10 can be tailored according to the operational requirements and limitations as further described in Section 3.1.3.

Decreasing the leakage reactance (X_E) of excitation transformer narrows the complex power regions of Fig. 10. If X_E=0, then each region will be shrunken to a line. Consequently, corresponding to each value of P_o, Q_R and Q_S each will have a single value.

Figure 10 also shows the complex powers at both line terminals obtained from detailed simulation of the study system, based on the use of the EMTP. Close agreement

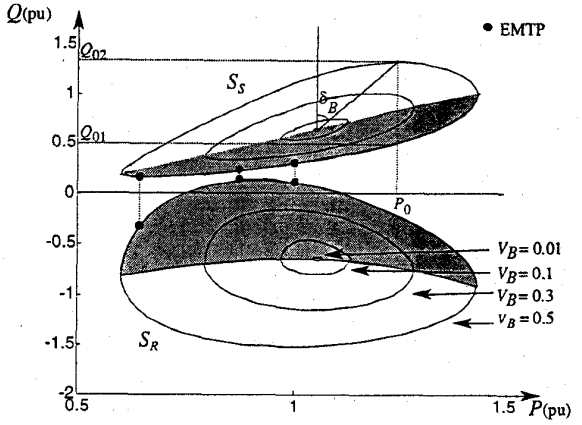

Figure 10: Impact of $|V_B|$ and δ_B on the sending-end (S_S) and the receiving-end(S_R) power (δ = 35°).

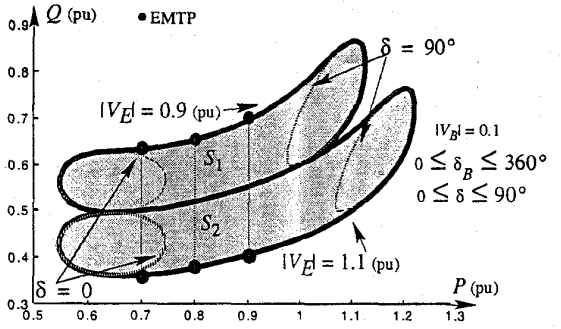

Figure 11: Effects of $|V_E|$ the on the complex power region of the sending-end .

between the corresponding results from the EMTP and the UPFC steady-state model (Fig. 8) verifies the accuracy of the developed steady-state model.

3.1.3 Case-3

If $\delta = \delta_S - \delta_R$ is varied from 0° to 90°, corresponding to each value of δ, a family of complex power regions S_S (or S_R), similar to that of Fig. 10, is obtained. All possible values of S_S (or S_R) can be identified by the closed-surface

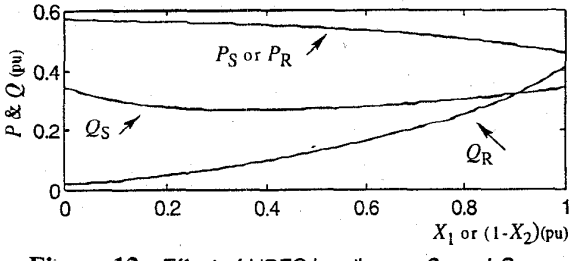

Figure 12: Effect of UPFC location on S_S and S_R.

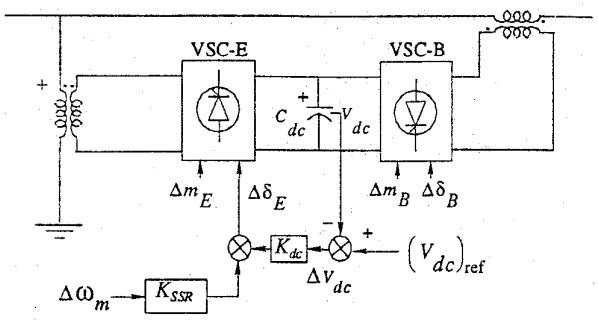

Figure 13: UPFC control strategy for SSR mitigation.

which encompasses all S_S (or S_R) regions. Figure 11 shows two such closed-surfaces corresponding to the sending end when $|V_E|$=0.9 per unit and $|V_E|$=1.1 per unit. Figure 11 also identifies complex power regions of the sending end

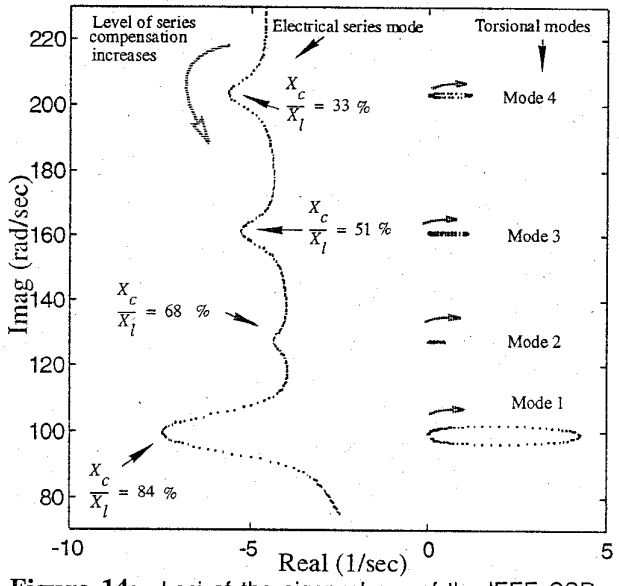

Figure 14: Loci of the eigenvalues of the IEEE SSR model. No SSR countermeasure in service.

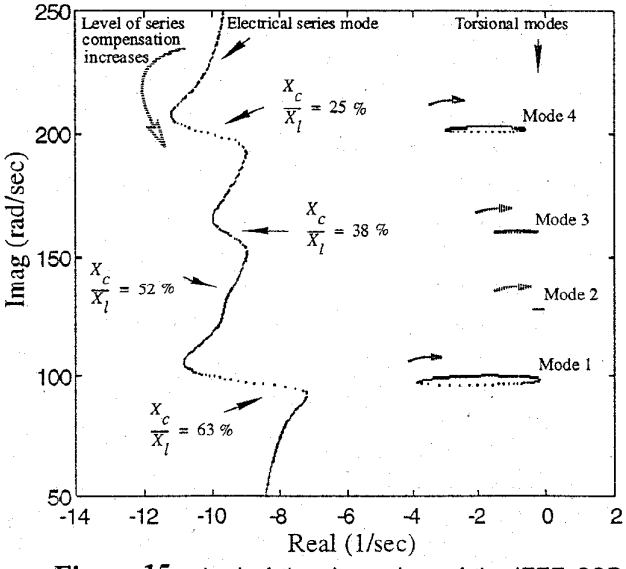

Figure 15: Loci of the eigenvalues of the IEEE SSR benchmark model when UPFC is used to mitigate torsional modes.

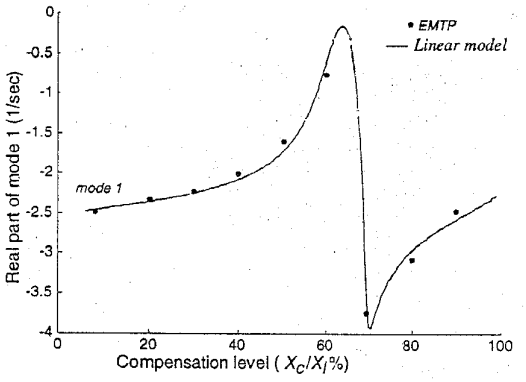

Figure 16: Real part of the eigenvalue of the first torsional mode.

for $\delta = 0°$ and $\delta = 90°$. Figure 11 indicates that for a given value of power transfer at a prespecified δ, the UPFC can readily control the reactive power requirement of the sending (and receiving) end. This is achieved by controlling $|V_E|$ through amplitude modulation index M_E of the boosting converter. Figure 11 also compares the results obtained from EMTP and the steady-state model.

3.1.4 Case-4

Figure 12 depicts the effect of the UPFC location on S_S and S_R when $|V_S| = |V_R| = |V_E| = 1.0$ per unit, $\delta = \delta_S - \delta_R = 35°$ and $|V_B| = 0.2$ per unit. Figure 12(a) indicates that when angle $\delta_B = 0°$, Q_R and Q_S are noticeably affected by the UPFC location.

3.2 Small-Signal Dynamics

The main purpose of this section is to verify the accuracy of the UPFC linearized model, equation (21), based on comparing eigen analysis results with the corresponding EMTP results. This section is also intended to demonstrate damping effect of the UPFC on torsional modes of power systems. The studies are conducted on the IEEE first benchmark model [7]. The UPFC is located at the sending-end after the generator step-up transformer.

3.2.1 Case-5

Figure 13 shows the UPFC control diagram to mitigate torsional oscillations. When no torsional countermeasure is in service, the first four torsional modes can become unstable as compensation level is varied from 0% to 100% [7]. Figure 14 shows loci of the system modes when the UPFC is not in service. Figure 14 clearly shows that the torsional modes, particularly mode 1, can become unstable. Figure 15 shows loci of the system modes when the UPFC is utilized to mitigate torsional modes. Torsional damping is achieved by modulating real power transfer through regulation of the dc link voltage. Comparison of Figs. 14 and 15 shows that the UPFC can effectively provide adequate damping for all torsional modes.

Figure 15 compares the real-part of the eigenvalue of the first mode obtained from the linearized model (Fig. 14) and the EMTP simulation of the study system. Close agreement between the corresponding results verifies the validity of the developed model. Since the linearized UPFC

model (equ. (21)) is deduced from the UPFC large-signal, dynamic model, equation (20), Figure 15 also is an indirect verification of the validity of the UPFC large-signal model.

4. CONCLUSIONS

This paper outlines a comprehensive and systematic approach for mathematical modelling of unified power flow controller (UPFC). Based upon the outlined approach, steady-state model, small-signal (linearized) dynamic model, and state-space, large-signal model of UPFC are developed. The models are applicable to power flow studies, eigen analysis, and transient stability investigations.

The developed formulation is general and independent of the pulse-width modulation (PWM) scheme used for the switching converters of the UPFC as long as fundamental frequency components of current and voltage are concerned.. The main assumption for developing the models is that power system is symmetrical and operates under three-phase balanced condition. This is the common assumption made for power flow, transient stability and eigen analysis of power systems. The developed procedures and models can be readily simplified and tailored for representation of GTO based static condensor (STATCON) and GTO based series capacitor.

Typical application examples of the developed models are also provided. The accuracy and validity of models are confirmed based on comparing the study results with those obtained from detailed time domain simulation, using the Electromagnetic Transients Program (EMTP).

5. REFERENCES

[1] L. Gyugyi, C.D. Schauder, S.L. Williams, T.R. Rietman, D.R. Torgerson, A. Edris, "The Unified Power Flow Controller: A New Approach to Power Transmission Control", IEEE Trans., Vol. PWRD-10, No. 2, pp. 1085-1097, April 1995.

[2] L. Gyugyi, "A Unified Power Flow Control Concept of r Flexible AC Transmission Systems", IEE Proceedings-C, Vol. 139, No. 4, pp. 323-333, July 1992.

[3] M.R. Iravani, P.L. Dandeno, K.H. Nguyen, D. Zhu, D. Maratukulam, "Applications of Static Phase Shifters in Power Systems", IEEE Trans., Vol. PWRD-9, No. 3, pp. 1600-1608, July 1994.

[4] M. Noroozian, G. Anderson, "Power Flow Control by Use of Controlled Series Components", IEEE Trans., Vol. PWRD-8, No. 3, pp. 1420-1429, July 1993.

[5] B.T. Ooi, S.Z. Dai, F.D. Galiana, "A Solid-State PWM Phase Shifter", IEEE Trans., Vol. 8, No. 2, pp. 573-579, April 1993.

[6] P.C. Krause, "Analysis of Electric Machinery", McGraw Hill, 1986.

[7] IEEE SSR Working Group, "First Benchmark Model for Computer Simulation of Subsynchronous Resonance", IEEE Trans., Vol. PAS-96, pp. 1565-1572, 1977.

Appendix A

Non-zero elements of matrix A_g, equ. (15):

$a_{g11}=a_{g22}=a_{g33}=-r_E/\ell_E, a_{g44}=a_{g55}=a_{g66}=-r_B/\ell_B,$
$a_{g17}=k_1\cos(\omega t+\delta_E), a_{g27}=k_1\cos(\omega t+\delta_E-120°),$
$a_{g37}=k_1\cos(\omega t+\delta_E-240°), a_{g47}=k_2\cos(\omega t+\delta_B),$
$a_{g57}=k_2\cos(\omega t+\delta_B-120°), a_{g67}=k_2\cos(\omega t+\delta_B-240°),$
$a_{g71}=k_3\cos(\omega t+\delta_E), a_{g72}=k_3\cos(\omega t+\delta_E-120°),$
$a_{g73}=k_3\cos(\omega t+\delta_E-240°), a_{g74}=k_4\cos(\omega t+\delta_B),$
$a_{g75}=k_4\cos(\omega t+\delta_B-120°), a_{g76}=k_4\cos(\omega t+\delta_B-240°),$
$k_1=-m_E/2\ell_E, k_2=m_B/2\ell_B, k_3=m_E/2C_{dc}, k_4=-m_B/2C_{dc}.$

Non-zero elements of matrix B_g, equ. (15):

$b_{g11}=b_{g22}=b_{g33}=1/\ell_E, b_{g44}=b_{g55}=b_{g66}=1/\ell_B, b_{g77}=1/C_{dc}$

Elements of vector F, equ. (17):

$$f_1=(|V_{Bt}||V_{Et}|/X_B)\sin(\delta_{Et}-\delta_{Bt})+(|V_{Bt}||V_{Et}|/X_E)\sin(\delta_{Et}-\delta_E)-(|V_{Et}||V_{Bt}|/X_B)\sin(\delta_{Et}-\delta B)$$

$$f_2=((X_E+X_B)/X_EX_B)|V_{Et}|^2-(|V_{Et}||V_{Bt}|/X_B)\cos(\delta_{Et}-\delta_{Bt})-[|V_{Et}||V_E|/X_E]\cos(\delta_{Et}-\delta_E)+(|V_{Et}||V_B|/X_B)\cos(\delta_{Et}-\delta_B)$$

$$f_3=(|V_{Et}||V_{Bt}|/X_B)\sin(\delta_{Bt}-\delta_{Et})+(|V_{Bt}||V_B|/X_B)\sin(\delta_{Bt}-\delta_B)$$

$$f_4=|V_{Bt}|^2/X_B+(|V_{Et}||V_{Bt}|/X_B)\cos(\delta_{Bt}-\delta_{Et})+(|V_{Bt}||V_B|/X_B)\cos(\delta_{Bt}-\delta_B)$$

Non-zero elements of matrix A_{dqo}, equ. (20):

$a_{11}=a_{22}=-R_E/\ell_E, a_{33}=a_{44}=-R_B/\ell_B, a_{12}=-a_{21}=a_{34}=-a_{43}=\omega, a_{15}=k_1\cos\delta_E, a_{25}=k_1\sin\delta_E, a_{35}=k_2\cos\delta_B, a_{45}=k_2\sin\delta_B, a_{51}=-(3k_3/2)\cos\delta_E, a_{52}=-(3k_3/2)\sin\delta_E, a_{53}=(3k_4/2)\cos\delta_B, a_{54}=(3k_4/2)\sin\delta_B$

Non-zero elements of matrix B_{dqo}, equ. (20):

$b_{11}=b_{22}=1/\ell_E, b_{33}=b_{44}=1/\ell_B, b_{55}=1/C_{dc}$

Non-zero elements of matrix A, equ. (21)

$a_{11}=a_{22}=-R_E\omega_o/\ell_E, a_{33}=a_{44}=-R_B\omega_o/\ell_B, a_{12}=-a_{21}=a_{34}=-a_{43}=\omega_o, a_{15}=k_5\cos\delta_E, a_{25}=k_5\sin\delta_E, a_{35}=k_6\cos\delta_B, a_{45}=k_6\sin\delta_B, a_{51}=k_7\cos\delta_E, a_{52}=k_7\sin\delta_E, a_{53}=k_8\cos\delta_B, a_{54}=k_8\sin\delta_B, k_5=-\omega_oM_E/2\ell_E, k_6=\omega_oM_B/2\ell_B, k_7=\omega_oM_E/2C_d, k_8=-\omega_oM_B/2C_d$

Non-zero elements of matrix B, equ. (21):

$b_{11}=-k_9V_d\cos\delta_E, b_{12}=k_9M_E\sin\delta_E, b_{21}=-k_9V_d\sin\delta_E, b_{22}=-k_9M_E\cos\delta_E, b_{33}=k_{10}V_d\cos\delta_B, b_{34}=-k_{10}M_B\sin\delta_B, b_{43}=k_{10}V_d\sin\delta_B, b_{44}=k_{10}M_B\cos\delta_B,$
$b_{51}=k_{11}(I_{Ed}\cos\delta_E+I_{Eq}\sin\delta_E),$
$b_{52}=-k_{11}M_E(I_{Ed}\sin\delta_E-I_{Eq}\cos\delta_E),$
$b_{53}=-k_{11}(I_{Bd}\cos\delta_B+I_{Bq}\sin\delta_B),$
$b_{54}=k_{11}M_B(I_{Bd}\sin\delta_B-I_{Bq}\cos\delta_B),$
$k_9=\omega_o/2\ell_E, k_{10}=\omega_o/2\ell_B, k_{11}=\omega_o/2C_d$

S.A. Nabavi-Niaki received his B.Sc. and M.Sc. degrees both in electrical engineering from Amirkabir University of Technology (Tehran Polytechnique) in 1987 and 1990 respectively. He is currently a Ph.D. student at the Department of Electrical and Computer Engineering at the University of Toronto. His research interests are power system control and modelling.

M.R. Iravani received his B.Sc. degree in electrical engineering from Tehran Polytechnic University in 1975, and M.A.Sc. and Ph.D. degrees from the University of Manitoba in 1981 and 1985 respectively. He worked as a consultant from 1976 to 1980. He was assistant professor at the University of Windsor from 1985 to 1987 when he joined the University of Toronto. Currently he is a professor in the Department of Electrical and Computer Engineering at the University of Toronto. His research interests are in the fields of power electronics and power system dynamics.